
Article:
Alexander, JA, Scheltens, FJ, Drummy, LF et al. (4 more authors) (2017) High-resolution monochromated electron energy-loss spectroscopy of organic photovoltaic materials. Ultramicroscopy, 180. pp. 125-132. ISSN 0304-3991

https://doi.org/10.1016/j.ultramic.2017.03.004

High-resolution monochromated electron energy-loss spectroscopy of organic photovoltaic materials

Jessica A. Alexander,[a] Frank J. Scheltens,[a] Lawrence F. Drummy,[b] Michael F. Durstock,[b] Fredrik S. Hage,[c] Quentin M. Ramasse,[c] and David W. McComb[a,*]

[a] Center for Electron Microscopy and Analysis, Department of Materials Science and Engineering, The Ohio State University, Columbus, OH, United States
[b] Materials and Manufacturing Directorate, Air Force Research Laboratory, Wright-Patterson Air Force Base, WPAFB, OH, United States
[c] SuperSTEM Laboratory, SciTech Daresbury Campus, Daresbury, United Kingdom

*Corresponding author.

Email address: mccomb.29@osu.edu

Keywords: electron energy-loss spectroscopy (EELS), scanning transmission electron microscopy (STEM), copper phthalocyanine (CuPc), C_{60}, poly(3-hexlythiophene) (P3HT), [6,6] phenyl-C_{61} butyric acid methyl ester (PCBM)

Abstract

Advances in electron monochromator technology are providing opportunities for high energy resolution (10 – 200 meV) electron energy-loss spectroscopy (EELS) to be performed in the scanning transmission electron microscope (STEM). The energy-loss near-edge structure in core-loss spectroscopy is often limited by core-hole lifetimes rather than the energy spread of the incident illumination. However, in the valence-loss region, the reduced width of the zero loss peak makes it possible to resolve clearly and unambiguously spectral features at very low energy-losses (< 3 eV). In this contribution, high-resolution EELS was used to investigate four materials commonly used in organic photovoltaics (OPVs): poly(3-hexlythiophene) (P3HT), [6,6] phenyl-C_{61} butyric acid methyl ester (PCBM), copper phthalocyanine (CuPc), and fullerene

(C_{60}). Data was collected on two different monochromated instruments – a Nion UltraSTEM 100 MC 'HERMES' and a FEI Titan^3 60-300 Image-Corrected S/TEM – using energy resolutions (as defined by the zero loss peak full-width at half-maximum) of 35 meV and 175 meV, respectively. The data was acquired to allow deconvolution of plural scattering, and Kramers-Kronig analysis was utilized to extract the complex dielectric functions. The real and imaginary parts of the complex dielectric functions obtained from the two instruments were compared to evaluate if the enhanced resolution in the Nion provides new opto-electronic information for these organic materials. The differences between the spectra are discussed, and the implications for STEM-EELS studies of advanced materials are considered.

1. Introduction

Organic photovoltaics (OPVs) have garnered research interest as an alternative to traditional inorganic solar cells due to their light weight, flexibility, and low manufacturing costs.[1] Although improvements in device technology has led to OPVs with power conversion efficiencies approaching 10%, extending their efficiency beyond this 10% barrier has proved challenging.[2] One cause for this stagnation is that little is known about the electronic structure and bonding of the donor/acceptor interface in OPV devices. While much work has been done to correlate device performance with the morphology of the donor/acceptor interface,[3-12] it is challenging to measure directly the opto-electronic properties of the donor/acceptor interface. This information is critical as current generation within OPVs is contingent upon *both* the morphology and the electronic structure of this interface. This knowledge, coupled with what is already known about the interface morphology, could lead to designing better performing OPVs.

We have recently demonstrated how the opto-electronic structure of OPV related materials

can be probed via valence electron energy-loss spectroscopy (EELS) measurements made in a scanning transmission electron microscope (STEM).[13] The complex dielectric function, ε (E), which can be utilized to determine single electron transitions and collective excitations, is calculated from the valence-loss spectrum ($\Delta E < 50$ eV).[14] The spatial resolution of valence-loss spectra is on the order of a few nanometers, depending on both the incident electron energy and the actual energy-loss.[15,16] Thus, by identifying which single electron transitions between bonding and anti-bonding sites are excited, it is possible to extract information about the local chemical environment in the material.[17]

In EELS, the zero loss peak (ZLP) is associated with electrons that have lost no energy (or very small amounts of energy) as they have passed through the sample, and the full-width at half-maximum (FWHM) of the ZLP is normally used as a measure of the spectral resolution. The implementation of electron monochromators in the scanning transmission electron microscope (STEM) has enabled EELS measurements to be performed with an energy resolution that matches, or improves on, the resolution that can be obtained using synchrotron-based X-ray absorption spectroscopy.[18] While this has benefits for core-loss spectroscopy, in particular for discrimination between energy-loss near-edge structure in mixed phase materials, the ionization edges are often limited in resolution by the core-hole lifetime rather than the energy resolution of the incident electron beam. However, the energy resolution of the incident beam has a much larger role in the analysis of valence-loss EELS data. The intensity of the ZLP at $1/10^{th}$, $1/100^{th}$ and $1/1000^{th}$ of the maximum is important as the intensity of the "tail" can mask spectral features at low energy-losses. By reducing this ZLP tail intensity, it is possible to measure, unambiguously, features at very low energy losses, including vibrational peaks in EEL spectra, as Krivanek et al.[18] have recently shown utilizing a Nion high-energy resolution monochromated

EELS system (HERMES) STEM.[19-21]

We have previously reported the results of our investigation of OPV materials using valence loss spectroscopy.[13] In this contribution, the effects of the tails of the ZLP on the energy-loss spectra of beam sensitive organic materials were studied to determine if additional information about the electronic structure of common OPV materials could be obtained using instruments with very high energy resolutions. EELS measurements made on a Nion UltraSTEM 100 MC HERMES have been compared with those from a FEI Titan^3 60-300 Image-Corrected S/TEM. EELS data were collected for copper phthalocyanine (CuPc), fullerene (C_{60}), poly(3-hexylthiophene) (P3HT), and [6,6] phenyl-C_{61} butyric acid methyl ester (PCBM) films. The goal was to establish the potential of monochromated STEM-EELS at the highest energy resolution for experiments measuring the complex dielectric function at the acceptor/donor interface of OPV devices.

2. Materials and methods

Four organic materials were studied in this work: copper phthalocyanine (CuPc), fullerene (C_{60}), poly(3-hexylthiophene) (P3HT), and [6,6] phenyl-C_{61} butyric acid methyl ester (PCBM). Thermal vapor deposition methods were utilized to prepare thin films (with thicknesses less than 50 nm) of CuPc, C_{60}, and PCBM (see Table 1 for growth parameters) on room temperature freshly cleaved rock salt substrates (NaCl and KCl with (100) orientation). The evaporation chamber was located within an argon-filled glove box. Thin films of P3HT were prepared by spin-coating a solution of P3HT in dichlorobenzene onto room temperature KCl substrates. These thin films were collected onto lacey carbon-coated TEM grids after they were floated off by dissolution of the substrates in distilled water.

Table 1: Growth parameters used for CuPc, C60, and PCBM thin films.

Material	Growth Rate (nm/min)	Pressure (torr)
CuPc	~ 1.7	~ 3 x 10^{-7}
C_{60}	~ 0.6	~ 6 x 10^{-7}
PCBM	~ 0.5	~ 4.5 x 10^{-6}

EELS measurements were acquired using similar beam conditions for two different microscopes: (1) a FEI Titan^3 60-300 Image-Corrected S/TEM and (2) a Nion UltraSTEM 100MC 'HERMES'. STEM-EELS experiments were conducted at 60 keV, in conjunction with procedures minimizing the amount of electron beam exposure, as these organic materials were susceptible to electron beam damage.[13] All of the microscope alignments and optimization of the EELS acquisition parameters were conducted on an area of the TEM grid that was not adjacent to any of the regions of interest on the grid. This ensured that the samples were not pre-exposed to the electron beam before collection of the data. Next, the edge of the thin film was brought into the field of view (~ 1 μm^2) for any final beam adjustments, after which the electron beam was blanked. The sample position was blindly adjusted to bring an area of the sample that had not been previously scanned into the field of view. While set to continuously scan the sample, the electron beam was unblanked, and the EELS acquisition was started. After conclusion of the EELS acquisition, the beam was blanked. EEL spectra acquired utilizing the FEI Titan^3 60-300 Image-Corrected S/TEM (hereafter referred to as 'Titan') and the attached Gatan Quantum spectrometer were collected in single-EELS mode with short acquisition times (2 – 4 ms). The convergence and collection semi-angles were 5 mrad and 15 mrad, respectively. This data were collected with a dispersion of 0.025 eV/channel, and the measured energy resolutions were in the

range of 0.17 – 0.20 eV. These short acquisition times resulted in noisy data, so multiple individual spectra were collected and summed together to improve the signal-to-noise ratio (SNR). The EELS spectra collected on the Nion UltraSTEM 100 MC HERMES (hereafter referred to as 'Nion') were acquired in dual-EELS mode using convergence and collection semi-angles of 34 mrad and 44 mrad, respectively. In this mode, two spectra were sequentially acquired at each pixel. The first spanned the range (-1 to 9 eV) that encompassed the ZLP (5 ms acquisition), and the second (~0.05 to 10 eV) covered the low energy-loss region (100 to 300 ms acquisition). By using a starting energy of ~0.05 eV for the second spectra, the most intense part of the ZLP was not collected to ensure that the ZLP did not saturate the detector during this data acquisition. These spectra were collected with a dispersion of 0.005 eV/channel, while the monochromator was adjusted to provide an acceptable compromise between beam current (and therefore signal-to-noise ratio) and energy resolution, resulting in a measured energy resolution of approximately 35 meV. Again, multiple spectra were summed together to improve the SNR. To enable the analysis required for obtaining the opto-electronic properties, single EELS spectra were also collected for the extended energy range of -5 to 35 eV. The effective energy resolution of these data sets was ~60 meV as they were limited by the point-spread function (PSF) of the detector as a result of the reduced energy dispersion (0.02 eV/channel) necessary to collect data for desired energy range.

3. Results and discussion

In Figure 1, the ZLPs collected *through* the CuPc specimen as well as a table comparing their widths at FWHM, FWQM (full-width at quarter-maximum) and FWTM are shown. The energy resolution on the Nion (best reported if 9-10 meV, 35 meV for the beam settings used for these

experiments as measured through the specimen) is better than on the Titan (best observed in our microscope is 50 meV, 175 meV for the beam settings used for these experiments as measured through the specimen) by a factor of five. This improvement in energy resolution makes it realistic to observe peaks at energy-losses below 1eV.

In order to compare the shape of the ZLP on both instruments, the Nion ZLP was numerically broadened to match the FWHM of the ZLP from the Titan (shown as the dashed green line on Figure 1). There is very good agreement between the shapes of the ZLPs on the two instruments. A small difference between this simulated ZLP and the ZLP from the Titan instrument is observed as a 10% change at FWQM and 15% at FWTM (Figure 1). Although the instruments have different monochromator designs – the Titan utilizes a Wien filter[22] and the Nion utilizes an alpha filter[19] – it is not obvious that this would contribute to this observed difference in zero-loss peak shape. The Titan data was recorded at a smaller dispersion (0.025 eV/channel) than on the Nion (0.005 eV/channel), but the EELS data collected on the Titan does not become limited by the PSF unless the dispersion used is 0.325 eV/channel or less (see Figure S1). Thus, the small difference in the two ZLPs could be due to differences in the higher-order spectrometer aberrations as the Nion is fitted with a modified Gatan Enfinium spectrometer while the Titan is fitted with a Gatan Quantum imaging filter.

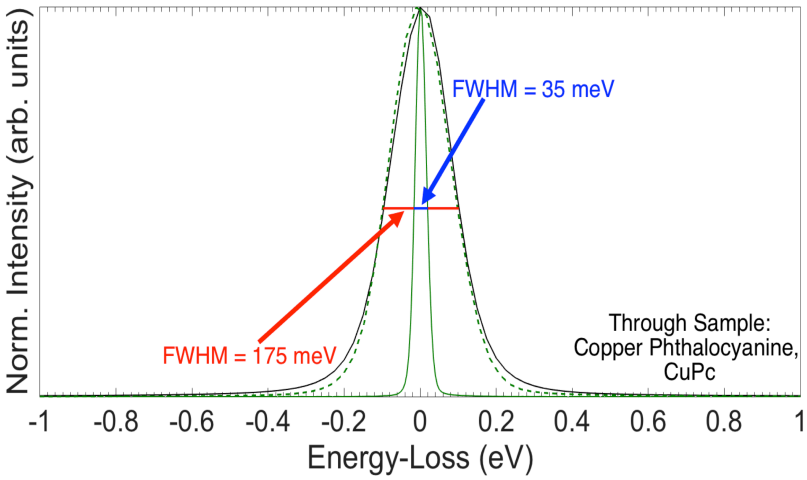

	FEI Titan³	Nion UltraSTEM	FEI Titan³/ Nion UltraSTEM	Normalized
FWHM	175 meV	35 meV	5.00	1
FWQM	275 meV	50 meV	5.50	1.1
FWTM	375 meV	65 meV	5.77	1.154

Figure 1: Comparisons between the ZLPs collected on the Nion (solid green) and the Titan (solid black). A theoretical ZLP with the same energy resolution as the Titan is shown for the Nion (dashed green). Additionally, specific values of FWHM, FWQM, and FWTM are compiled (see table).

The spectra collected prior to zero-loss subtraction from each microscope are shown in Figure 2. It is apparent that some of the low energy spectral features are unambiguously determined in the Nion data due to the reduced FWHM of the ZLP. For example, the features indicated by red arrows (Figure 2) – in C_{60} at 2 eV; in PCBM at 2.5 eV; in P3HT at 2.6 eV – appear as shoulders on the ZLP in the Titan data, whereas they are more clearly defined as distinct peaks in the Nion data. In the CuPc data, the features in the range 6 – 8 eV, indicated by the blue arrows (Figure 2), are also more defined in the Nion data.

While it is possible to identify the spectral features more readily in the Nion data, it is interesting to note that, with one exception, there are no new features in the Nion data – every

peak can be identified in the data from both microscopes. The exception is the peak at ~360 meV in the spectrum collected from CuPc on the Nion (Figure 3). This peak is present in the EEL spectra collected from all four materials, although the center energy ranges from 250 meV to 400 meV. For the materials in which the peak is centered at about 400 meV, this low energy-loss feature could be attributed to an O-H bond stretching mode,[23] although it might also have overlapping contributions from C-C and C-H vibrational modes, and it is these C-C and C-H modes which are likely measured in the lower energy vibrational peaks. In summary, these qualitative comparisons illustrate how the improved resolution of the Nion, as compared to that of the Titan, makes it easier to definitively identify spectral features, especially weak peaks at very low energy-losses.

The intensity of the inelastic signal in energy-loss spectroscopy is greatest in the valence-loss region which means that valence-loss spectroscopy has enormous potential for beam-sensitive materials, such as those found in polymers, composites, biomaterials, and OPVs. Furthermore, since the complex dielectric function can be extracted from the valence loss spectrum, it is possible to obtain information about the optical and electronic properties of the material with nanometer scale spatial resolution. We have reported previously on the use of this technique to obtain the optical properties of OPV materials.[13] The next step in the comparison of the Nion and Titan data is to compare the real and imaginary parts of the complex dielectric function to determine the impact of the improved energy resolution of the Nion. There are three steps to achieve this: (1) fitting and subtraction of the ZLP, (2) deconvolution to remove plural scattering and obtain the single scattering distribution (SSD), and (3) Kramers-Kronig (KK) analysis of the SSD to obtain the complex dielectric function. The deconvolution and KK routines require continuous data sets that span an energy range that is large enough to include the

majority of the inelastic scattering and that allows the fitting of a function to extend the data to high energy loss. As discussed below this creates significant challenges when the data are acquired with very high energy dispersion.

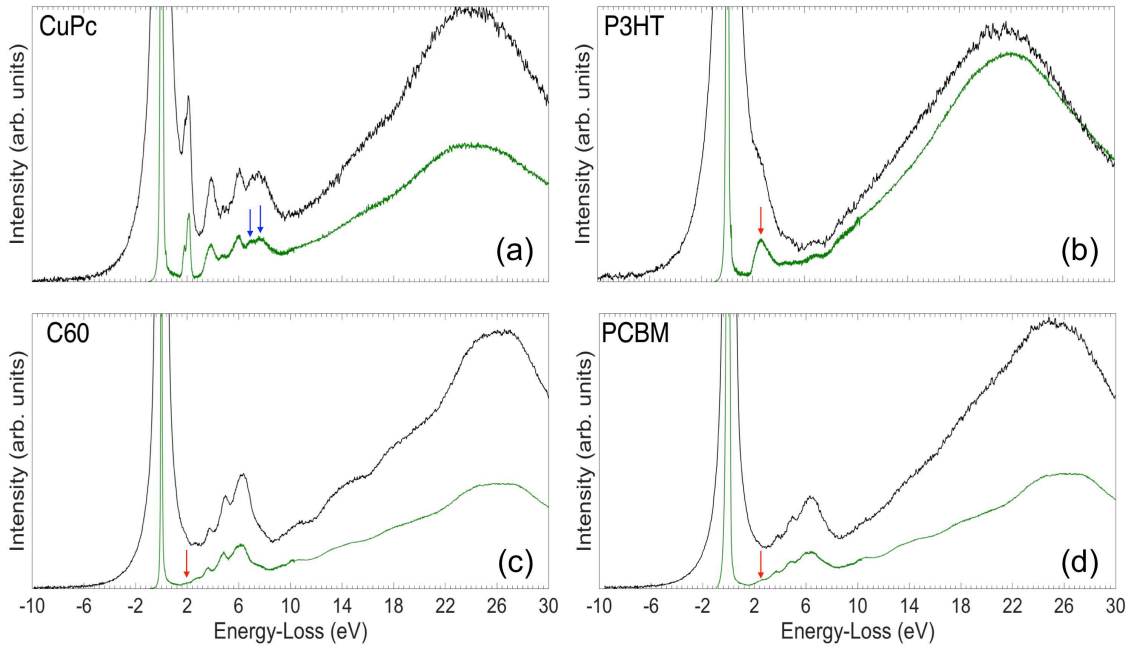

Figure 2: Comparison of energy-loss spectra collected on the Nion (green) and the Titan (black) for (a) CuPc, (b) P3HT, (c) C_{60}, and (d) PCBM.

The ZLP from the collected spectra was removed using the reflected tail method in Gatan's DigitalMicrograph software.[24] In principle, the partial ZLP on the negative (energy-gain) side of zero energy is "reflected" onto the energy-loss side and fitted in a defined energy window and spliced into the experimental spectrum. For the data collected on the Titan, this was straightforward. The spectra were collected with an extended negative energy range (-10.0 eV) to ensure that there was sufficient energy range to fit ZLP accurately, and the splicing point on the

energy-loss side was adjusted to ensure that any artifacts at the splicing point did not coincide with spectral regions of interest.

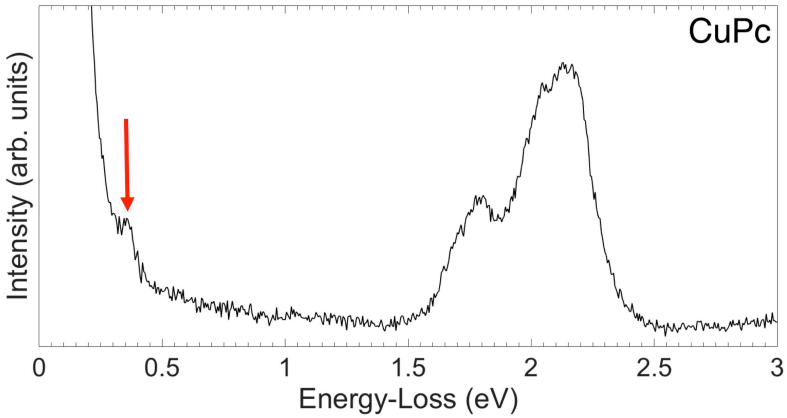

Figure 3: Nion CuPc spectrum displaying the peak attributed to an O-H bond stretch (at about 0.36 eV).

However, due to the high dispersion of the Nion data, the ZLP extraction process was less straightforward for these spectra. Since the data were collected in dual-EELS mode, the splicing tool in Gatan's DigitalMicrograph software was used to merge together the full ZLP (Figure 4a) with the low-loss (~0.05 to 10 eV) spectrum (Figure 4b). However, this made the reflected tail method for ZLP extraction impossible due to the poor signal-to-noise ratio (SNR) on the energy gain side of the ZLP (Figure 4c). This is a result of the short acquisition times used during the data collection for spectra that included the ZLP. This poor SNR compromised the ZLP extraction routine (Figure 4d), as the tail from the left side of the ZLP was not accurately reflected onto the right side of the ZLP.

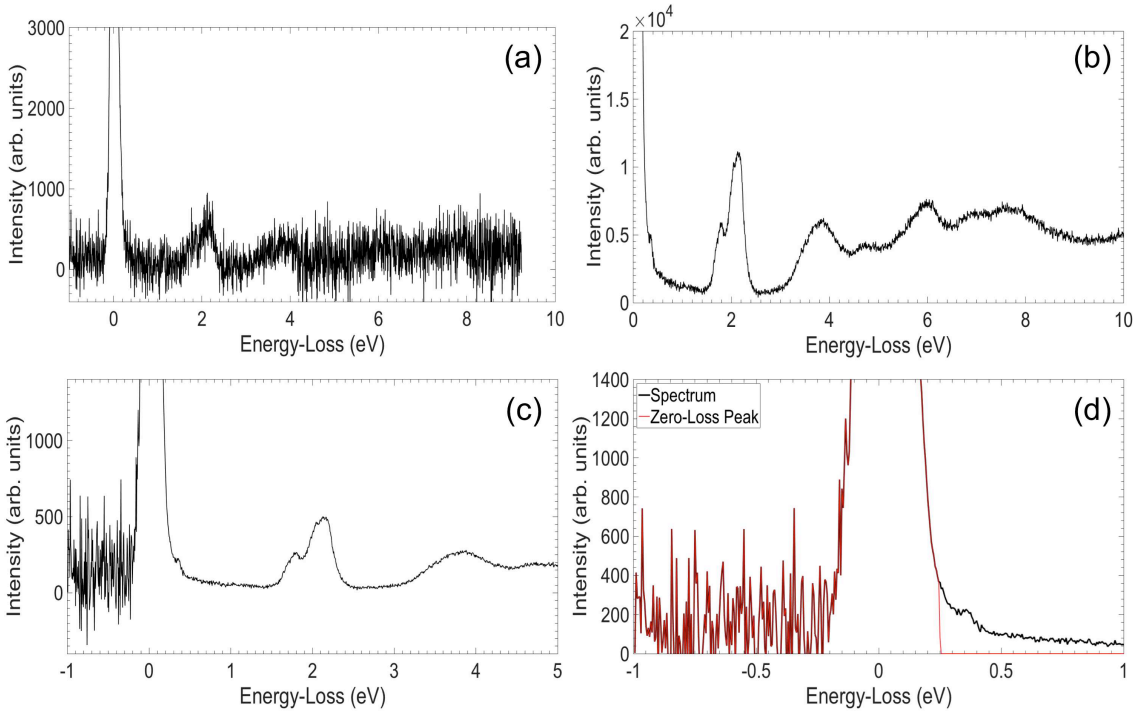

Figure 4: The (a) ZLP and (b) high-resolution low-loss spectra collected in dual-EELS mode on the Nion for CuPc. These two spectra were spliced together, which resulted in the spectrum in (c). Due to the large noise signal on the left side of the ZLP in (c), the ZLP extraction routine did not work properly (d).

To overcome the issues in the Nion data, a modified Voight function was used to fit the shape of the tail on the negative (energy-gain) side of the experimental ZLP:

$$f(\Delta E) = \frac{2ab\sqrt{\frac{4\ln(2)}{\pi}}\, e^{-4\ln(2)*(\Delta E)^2}}{\pi c\,(4(\Delta E)^2 + b^2)}$$

where a, b, and c are fitting coefficients, and ΔE is the energy-gain. After fitting the tail, the noisy data on the left side of the ZLP was replaced with the smoothed data from the fit. This fit was conducted on the experimental ZLP data up to -0.06 eV, as this was the highest energy that exhibited more intensity from noise rather than signal. The result of this fit is shown in Figure 5a

for CuPc. The region with poor SNR on the left side of the experimental ZLP was replaced with the smoothed fit which then allowed removal of the ZLP from the experimental data using the previously described reflected tail method. Figure 5 shows the successful ZLP extractions for the CuPc EELS data collected on the (b) Titan and (c) Nion. In both spectra, the tails are accurately reflected from the left side of the ZLP to the right. This process was repeated for all four materials.

In order to perform the deconvolution step to remove plural scattering and obtain the single scattering distribution (SSD), the energy-loss spectra need to extend to an energy-loss significantly beyond that of the plasmon peak (the broad peak at ~20 to 30 eV associated with collective oscillations of the valence electrons). This is necessary to meet the requirement that the experimental spectrum falls almost to zero intensity at both ends of the energy-loss range to avoid "ringing" artefacts in the application of the discrete Fourier transform.[14] This constraint is easily met on the low (energy-gain) side of the ZLP. At finite energy-losses it is necessary to numerically extrapolate the data to high energy-loss. This is straightforward if the experimental spectrum has been recorded up to an energy-loss beyond that of all collective excitations so that a smooth monotonic function can be fitted and extrapolated using routines in DigitalMicrograph. This is the case for the Titan data as the low-loss spectra were recorded to approximately 40 eV since the resolution was not point-spread limited in the conditions used i.e. ΔE=175 meV. However, as mentioned in the methods section, to obtain the high-resolution (ΔE=35 meV) data on the Nion, the low-loss spectra could only be collected to approximately 10 eV. Thus, it was necessary to splice this spectrum with the lower resolution data recorded over an extended energy range (-5 to 35 eV). Since these data were collected at a lower dispersion to accommodate for the larger collected energy range, it was necessary to interpolate the spectra to

match the dispersion of the low-loss spectra. This interpolated extended energy-loss spectrum was then spliced with the low-loss spectrum at approximately 10 eV. This resulted in a final spectrum consisting of the high-resolution low-loss data from -1 to 10 eV and of the interpolated extended low-loss data from 10 to 35 eV.

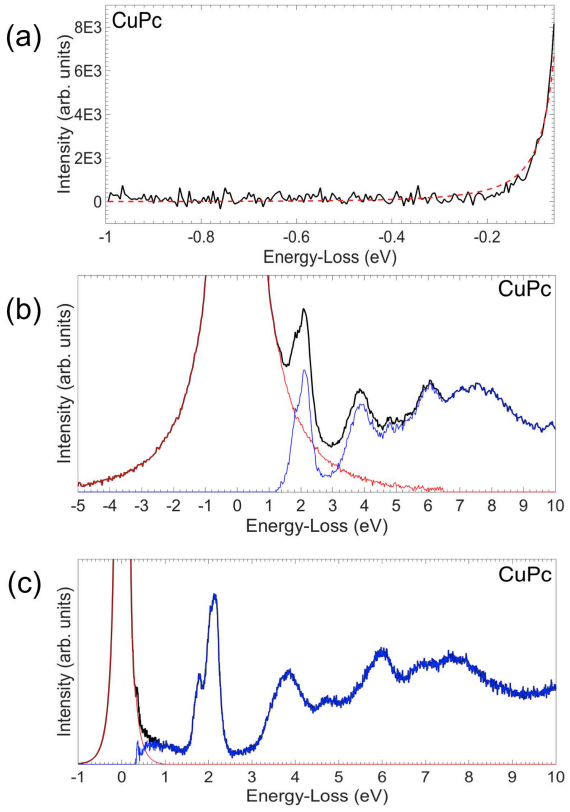

Figure 5: (a) Results of fitting the tails of the ZLP for the Nion CuPc data. As is shown, the fitted function (red dashed line) models the experimental (black line) well. (b) Successful ZLP extractions for data collected on the Titan and the (c) Nion for CuPc. The black, red, and blue lines denote the raw data, zero-loss peak, and inelastic spectra, respectively.

The complex dielectric function, $\varepsilon(E)$, is a causal function[25] that is related to the SSD, $J^l(E)$, as:[14]

$$J^1(E) \propto \mathrm{Im}\left[\frac{-1}{\varepsilon(E)}\right]$$

Thus, the SSD can be analyzed via a Kramers-Kronig transformation to determine Re [1/ε(E)] from Im [1/ε(E)].[25] The real and imaginary parts of the complex dielectric function (ε_1 and ε_2, respectively) were calculated as:[14]

$$\varepsilon(E) = \varepsilon_1(E) + i\varepsilon_2(E) = \frac{\mathrm{Re}\left[1/\varepsilon(E)\right] + i\ \mathrm{Im}\left[-1/\varepsilon(E)\right]}{\left(\mathrm{Re}\left[1/\varepsilon(E)\right]\right)^2 + \left(\mathrm{Im}\left[-1/\varepsilon(E)\right]\right)^2}$$

ε_1 and ε_2 were obtained from each of the EELS spectra collected using the Kramers-Kronig analysis routine in DigitalMicrograph. Figures 6 and 7 shows these resulting real (ε_1) and imaginary (ε_2) parts of the dielectric function, respectively, for each of the materials investigated.

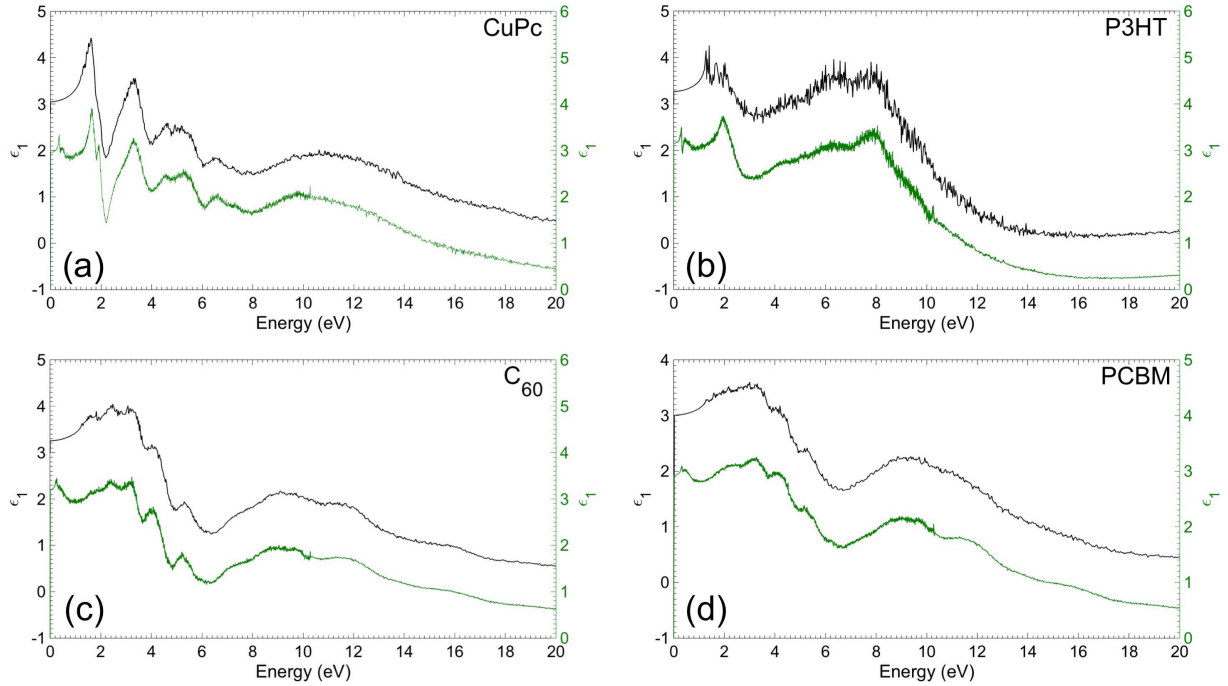

Figure 6: The ε_1 spectra collected on the Nion (green) and the Titan (black) for (a) CuPc, (b) P3HT, (c) C_{60}, and (d) PCBM. Comparisons of these spectra show that no new peaks are observable in the Nion data.

The ε_1 plots are generally in good agreement for the two instruments, but the data collected on the Nion is better resolved (Figure 6). For instance, in the CuPc ε_1 plot from the Nion data, there are two defined peaks at approximately 1.5 – 2.0 eV, whereas the second peak appeared to be just a shoulder on the right of the primary peak in the Titan data set. A similar observation can be made for the C_{60} ε_1 data in which the two distinct peaks in the Nion spectrum at approximately 2.75 eV appeared to be just one broad peak in the data collected on the Titan. There is also better definition in the Nion ε_1 spectra for PCBM (see the two peaks at approximately 2.5 eV) and P3HT (see the peak at 2.0 eV).

The imaginary, ε_2, part of the dielectric function can be directly related to single electron transitions between the valence and conduction bands in the material. These comparisons between the ε_2 spectra should highlight any new electronic information obtained as a result of the improved energy resolution of the Nion. Again, measurements on the Nion resulted in slightly better resolved peaks (Figure 7). However, in the CuPc ε_2 spectrum collected on the Nion, the relative intensities of the two peaks at approximately 2.0 eV are reversed. The relative intensities in the Nion data are in good agreement with optical ellipsometry data available in the literature.[26] It is probable that the reversal in peak intensities in the Titan data is due to errors in the ZLP extraction. It is possible that all of the intensity due to the ZLP's tail was not actually removed from the spectrum, which would have resulted in excess intensity in the low energy range of the inelastic spectrum. However, for all four materials there are no new peaks observed in any of the ε_2 plots and the assignment of features to single electron transitions is unchanged from an earlier analysis.[13] This would be expected, as the native line widths of the features in the low-loss spectra are broader than the energy resolution of the ZLP. However, the advantage in

monochromating the electron beam is that more separation is observed between closely spaced features in the spectra. While, at least for these OPV materials, there is little advantage to collecting data on the Nion other than simplifying the data analysis, comparisons between the Nion and Titan data sets exemplify how the monochromator is critical for observing features that are closely spaced together.

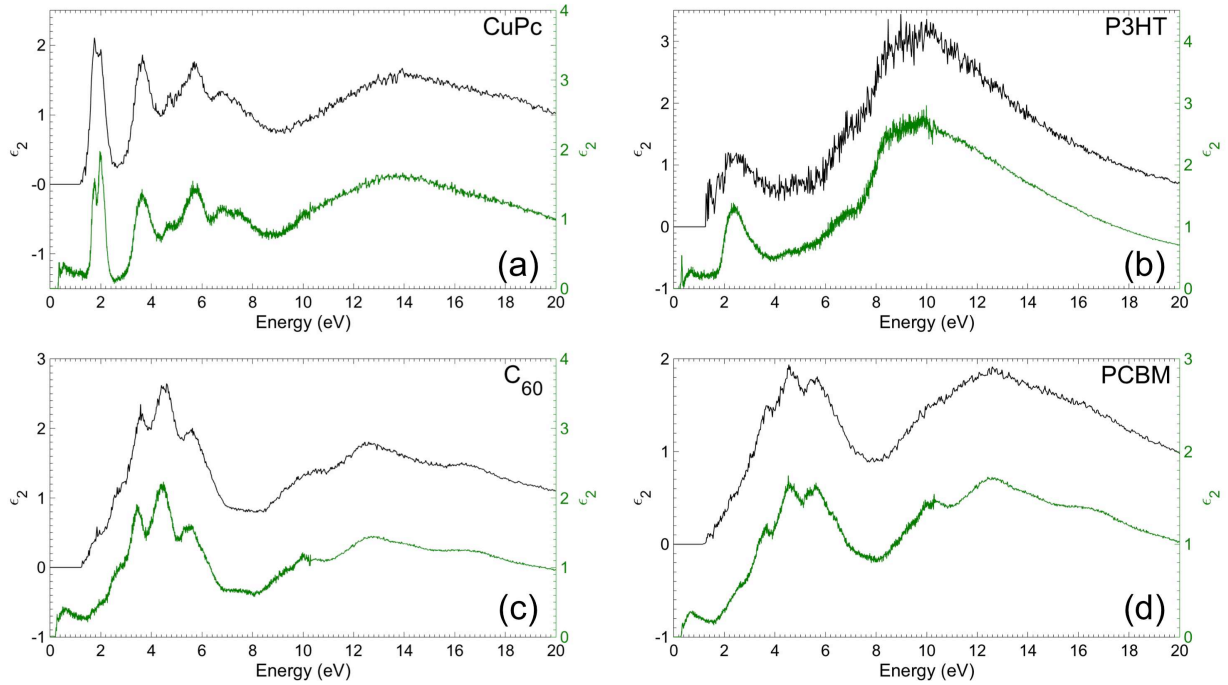

Figure 7: The ε_2 spectra collected on the Nion (green) and the Titan (black) for (a) CuPc, (b) P3HT, (c) C_{60}, and (d) PCBM. Comparisons of these spectra show that no new peaks are observable in the Nion data.

To be more quantitative in the comparison between the Titan and Nion data sets, the absorption coefficient, α, was extracted from the EELS data for all four materials. The absorption coefficient is related to the extinction coefficient, κ, as $\alpha = 4\pi\kappa/\lambda$ where λ is the wavelength. Furthermore, κ is related to ε_1 and ε_2 as $\varepsilon_1 = n^2-\kappa^2$ and $\varepsilon_2 = 2n\kappa$ where n is the refractive index. It is important to note that α is dependent on *both* ε_1 and ε_2. Figure 8 shows the extracted plots of

absorption coefficient as a function of energy-loss for both the Titan and Nion data for all four materials. There is extremely good agreement between these data sets. Additionally, the inversion of the relative intensities of the first two peaks in the CuPc is no longer observed, which can be attributed to the fact that α depends not only on ε_2, but also on ε_1.

Overall, these plots show that monochromated STEM-EELS is a very powerful approach to making spatially resolved measurements of the absorption coefficient, even in beam sensitive organic materials.

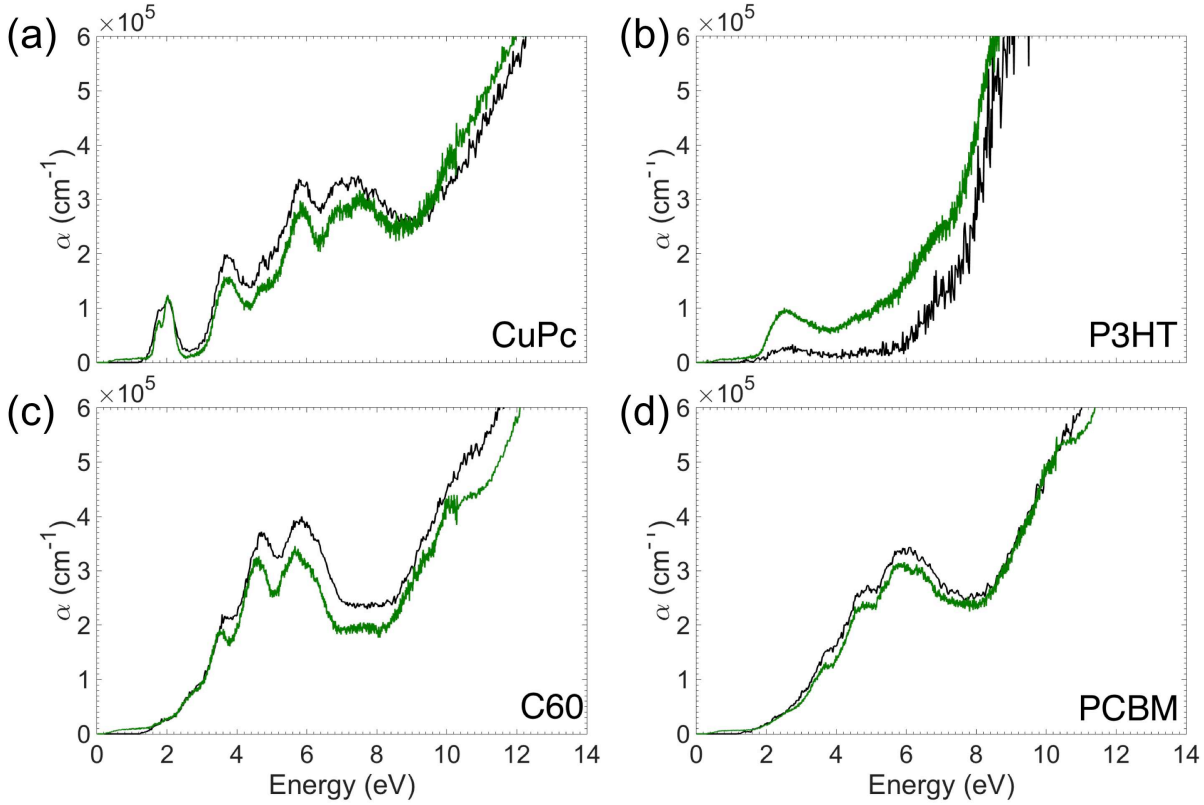

Figure 8: The α spectra determined from EELS data collected on the Nion UltraSTEM (green) and the FEI Titan[3] (black) for (a) CuPc, (b) P3HT, (c) C_{60}, and (d) PCBM.

4. Conclusions

In this work, EELS spectra were collected on two monochromated scanning transmission electron microscopes with differing energy resolution capabilities for CuPc, C_{60}, P3HT, and PCBM. The superior energy resolution of the Nion UltraSTEM 100 MC 'HERMES' microscope (35 meV energy resolution in the beam conditions used here) improved the resolution of the peaks in the raw spectra and made it possible to measure spectral features below 2 eV, including an O-H bond stretch at approximately 0.4 eV. However, for the materials being investigated no new peaks were measured in the imaginary part of the complex dielectric function, indicating that, for these specific materials, the data collected on an FEI Titan^3 60-300 Image-Corrected S/TEM (175 meV energy resolution in the beam conditions used here) can be processed to obtain the same electronic information as for data collected on the Nion. We have demonstrated how monochromated STEM-EELS data can be manipulated to extract the absorption coefficient. It is concluded that monochromated STEM-EELS in the valence loss region shows great promise for determining optical properties with high spatial resolution even in beam sensitive materials.

Acknowledgements

This paper is dedicated to Dr. Ondrej Krivanek. His work on electron spectrometers and electron monochromators has had a major influence on the use of electron energy-loss spectroscopy in the microscopy community and has opened many opportunities for investigation of new materials and phenomena. The authors would like to thank all collaborators and technical support at both the Center for Electron Microscopy (CEMAS) at The Ohio State University and the Materials and Manufacturing Directorate at the Air Force Research Laboratory (AFRL) at Wright-Patterson Air Force Base. Funding was provided by an AFRL/DAGSI Ohio-Student Faculty Research Fellowship awarded by the Air Force Laboratory Manufacturing and Materials

Directorate, and by The Ohio State University through a Distinguished University Fellowship. The SuperSTEM Laboratory is the U.K. National Facility for Aberration-Corrected Scanning Transmission Electron Microscopy, supported by the Engineering and Physical Sciences Research Council (EPSRC).

References

1. C.J. Brabec, A. Cravino, D. Meisser, N.S. Sariciftci, T. Fromherz, M.T. Rispens, L. Sanchez & J.C. Hummelen. Origin of the open circuit voltage of plastic solar cells. *Adv. Funct. Mater.* **11,** 374-380 (2001).
2. R.F. Service. Outlook brightens for plastic solar cells. *Science* **332,** 293 (2011).
3. D. Chen, A. Nakahara, D. Wei, D. Nordlund & T.P. Russell. P3HT/PCBM bulk heterojunction organic photovoltaic: correlating efficiency and morphology. *Nano Lett.* **11,** 561-567 (2011).
4. M. Pfannmöller, H. Flugge, G. Benner, I. Wacker, C. Sommer, M. Hanselmann, S. Schmale, H.Schmidt, F.A. Hamprecht, T. Rabe, W. Kowalsky & R.R. Schroder. Visualizing a homogeneous blend in bulk:heterojunction polymer solar cells by analytical electron microscopy. *Nano Lett.* **11,** 3099-3107 (2011).
5. M. Pfannmöller, H. Flugge, G. Benner, I. Wacker, W. Kowalsky & R.R. Schroder. Visualizing photovoltaic nanostructures with high-resolution analytical electron microscopy reveals material phases in bulk heterojunctions. *Synth. Met.***161,** 2526-2533 (2012).
6. L.F. Drummy, R.J. Davis, D.L. Moore, M. Durstock, R.A. Vaia & J.W.P. Hsu. Molecular-scale and nanoscale morphology of P3HT:PCBM bulk heterojunctions: energy-filtered TEM and low-dose HREM. *Chem. Mater.* **23,** 907-912 (2011).

7. SS. van Bavel, M. Barenklau, G. de With, H.Hoppe & J. Loos. P3HT/PCBM bulk heterojunction solar cells: impact of blend composition and 3D morphology on device performance. *Adv. Funct. Mater.* **20,** 1458-1463 (2010).

8. B.V. Andersson, S. Masich, N. Solin & O. Inganäs. Morphology of organic electronic materials imaged via electron tomography. *J. Microsc.* **247,** 277-287 (2012).

9. B.V. Andersson, A. Herland, S. Masich & O. Inganäs. Imaging of the 3D nanostructure of a polymer solar cell by electron tomography. *Nano Lett.* **9,** 853-855 (2009).

10. S. van Bavel, E. Sourty, G. de With, K. Frolic & J. Loos. Relation between photoactive layer thickness, 3D morphology, and device performance in P3HT/PCBM bulk-heterojunction solar cells. *Macromolecules* **42,** 7396-7403 (2009).

11. S.S. van Bavel, E. Sourty, G. de With & J. Loos. Three-dimensional nanoscale organization of bulk heterojunction polymer solar cells. *Nano Lett.* **9,** 507-513 (2009).

12. J.B. Gilchrist, T.H. Basey-Fisher, S.C. Chang, F. Scheltens, D.W. McComb & S. Heutz. Uncovering the buried interface in organic solar cells. *Adv. Funct. Mater.* **24,** 6473-6483 (2014).

13. J.A. Alexander, F.J. Scheltens, L.F. Drummy, M.F. Durstock, J.B. Gilchrist, S. Heutz & D.W. McComb. Measurement of optical properties in organic photovoltaic materials using monochromated electron energy-loss spectroscopy. *J. Mater. Chem. A* **4,** 13636-13645 (2016).

14. R.F. Egerton. *Electron Energy-Loss Spectroscopy in the Electron Microscope.* (Springer, 2011).

15. R.F. Egerton. New techniques in electron energy-loss spectroscopy and energy-filtered imaging. *Micron* **34,** 127-139 (2003).

16. R.F. Egerton. Limits to the spatial, energy and momentum resolution of electron energy-loss spectroscopy. *Ultramicroscopy* **107**, 575-586 (2007).

17. A.M. Lesk. *Introduction to Symmetry and Group Theory for Chemists.* (Kluwer Academic Publishers, 2004).

18. O.L. Krivanek, T.C. Lovejoy, N. Dellby, T. Aoki, R.W. Carpenter, P. Rez, E. Soignard, J. Zhu, P.E. Batson, M.J. Lagos, R.F. Egerton & P.A. Crozier. Vibrational spectroscopy in the electron microscope. *Nature* **514,** 209-212 (2014).

19. O.L Krivanek, J.P. Ursin, N.J. Bacon, G.J. Corbin, N. Dellby, P. Hrncirik, M.F. Murfitt, C.S. Own & Z.S. Szilagyi. High-energy-resolution monochromator for aberration-corrected scanning transmission electron microscopy/electron energy-loss spectroscopy. *Phil. Trans. R. Soc. A*. **367,** 3683-3697 (2009).

20. O.L. Krivanek, T.C. Lovejoy, N. Dellby, & R.W. Carpenter. Monochromated STEM with a 30 meV-wide, atom-sized electron probe. *Microscopy* **62,** 3-21 (2013).

21. O.L. Krivanek, T.C. Lovejoy, M.F. Murfitt, G. Skone, P.E. Batson & N. Dellby. Towards sub-10 meV energy resolution STEM-EELS. *J. of Phys.: Conference Series* **522,** 012023 (2014).

22. P.C. Tiemeijer. Operation modes of a TEM monochromator. *Proc. EMAG '99, Sheffield.* Institute of Physics Conference Series, no. 161, pp. 191-194. Bristol, UK: Institute of Physics (1999).

23. D.M. Carey & G.M. Korenowski. Measurement of the Raman spectrum of liquid water. *J. Chem. Phys.* **108,** 2669-2675 (1998).

24. DigitalMicrograph EELS Analysis User's Guide. (2003).

25. D.W. Johnson. A Fourier series method for numerical Kramers-Kronig analysis. *J. Phys. A Math. Gen.* **8,** 490–496 (1975).

26. D. Datta, V. Tripathi, P. Gogoi, S. Banerjee & S. Kumar. Ellipsometric studies on thin film CuPc:C60 blends for solar cell applications. *Thin Solid Films.* **516,** 7237-7240 (2008).